Int. J. Therm. Sci. (2000) 39, 265–272

S1290-0729(00)00244-1/FLA

Unsteady free convection MHD flow past a vertical cylinder with heat and mass transfer

Periyana Gounder Ganesan *, Ponnamma Hari Rani

Department of Mathematics, Anna University, Chennai 600 025, India

(Received 6 June 1999, accepted 20 August 1999)

Abstract — Heat and mass transfer characteristics and the flow behavior on the MHD flow past a vertical cylinder are studied. The equations of conservation of mass, momentum, energy and concentration which govern the flow and heat and mass transfer are obtained. The nondimensional governing equations are solved by an efficient, more accurate, unconditionally stable and fast converging implicit scheme. The unsteady effects of material parameters such as Prandtl number, Schmidt number, buoyancy ratio parameter and magnetic parameter on the velocity, temperature and concentration are discussed. The local and average skin-friction, Nusselt number and Sherwood number are also presented graphically. The numerical predictions have been compared with the existing information in the literature and good agreement is obtained. © 2000 Éditions scientifiques et médicales Elsevier SAS

transient / free convection / MHD / heat and mass transfer / cylinder

Nomenclature

B_0	magnetic field strength	$kg{\cdot}s^{-2}{\cdot}A^{-1}$
C'	species concentration	$mol{\cdot}m^{-3}$
C	dimensionless species concentration	
Gr	thermal Grashof number	
Gr^*	mass Grashof number	
g	acceleration due to gravity	$m{\cdot}s^{-2}$
M	magnetic parameter	
N	combined buoyancy ratio parameter	
$\overline{Nu}$	dimensionless average Nusselt number	
Nu_x	dimensionless local Nusselt number	
Pr	Prandtl number	
r	radial coordinate measured from axis of cylinder	m
r_0	radius of cylinder	m
R	dimensionless radial coordinate	
Sc	Schmidt number	
$\overline{Sh}$	dimensionless average Sherwood number	
Sh_x	dimensionless local Sherwood number	
T'	temperature	K
T	dimensionless temperature	
t'	time	s
t	dimensionless time	
u, v	velocity components in x, r directions, respectively	$m{\cdot}s^{-1}$
U, V	dimensionless velocity components in X, R directions, respectively	
x	axial coordinate measured vertically upward	m
X	dimensionless axial coordinate	

Greek symbols

α	thermal diffusivity	$m^2{\cdot}s^{-1}$
β	volumetric coefficient of thermal expansion	K^{-1}
β^*	volumetric coefficient of expansion with concentration	$m^3{\cdot}mol^{-1}$
Δt	grid size in time	
ΔR	grid size in radial direction	
ΔX	grid size in axial direction	
ν	kinematic viscosity	$m^2{\cdot}s^{-1}$
ρ	density	$kg{\cdot}m^{-3}$
σ	electrical conductivity of the fluid	$kg^{-1}{\cdot}m{\cdot}s^3{\cdot}A^2$
τ_X	dimensionless local skin-friction	
$\bar{\tau}$	dimensionless average skin-friction	

Subscripts

w	conditions on the wall
∞	free stream condition

* Correspondence and reprints.
ganesan@annauniv.edu

i designates grid point along the X-direction
j designates grid point along the R-direction

Superscript

k time step level

1. INTRODUCTION

The study of flow problems, which involve the interaction of several phenomena, has a wide range of applications in the field of science and technology. One such study is related to the effects of free convection MHD flow, which plays an important role in agriculture, engineering and petroleum industries. The problem of free convection under the influence of a magnetic field has attracted the interest of many researchers in view of its application in geophysics and in astrophysics. The problem under consideration has important applications in the study of geological formations; in the exploration and thermal recovery of oil; and in the assessment of aquifers, geothermal reservoirs and underground nuclear waste storage sites. Results obtained from this study will be helpful in the prediction of flow, heat transfer and solute or contaminant dispersion about intrusive bodies such as salt domes, magnetic intrusions, piping and casting systems.

Agrawal et al. [1] discussed thermal and mass diffusion on hydromagnetic visco-elastic natural convection past an impulsively started infinite plate in the presence of a transverse magnetic filed. Helmy [2] studied the unsteady laminar free convection flow of an electrically conducting fluid through a porous medium bounded by an infinite vertical plane surface of constant temperature. Jones et al. [3] developed a new implicit algorithm for solving the time dependent, non-ideal magnetohydrodynamic equations. Shanker and Kishan [4] presented the effect of mass transfer on the MHD flow past an impulsively started infinite vertical plate. The authors [1–4] have given an importance to MHD flow past a vertical plate. The effects of heat and mass transfer on the natural convective flow along a vertical cylinder were studied by Chen and Yuh [5].

An analysis is made by Goldstein and Briggs [6] for the transient free-convection, heat transfer problem from vertical circular cylinders to a surrounding initially quiescent fluid. The transient is initiated by a change in wall temperature of the cylinder. The solutions for the velocity and penetration distance profiles for vertical cylinders with a step change in surface heat flux for arbitrary Prandtl number are given. Dring and Gebhart [7] presented experimental results for the transient average temperature of Nichrome wires in silicone oils and in air. They also compared their experimental results with pure conduction results and with a simplified quasistatic theory that yields a simple exponential solutions for the temperature response. Even for air, the conduction solution was found to be better than that predicted by this theory.

An experimental and analytical study is reported by Evans et al. [8] for transient natural convection in a vertical cylinder. The vertical cylinder is subjected to a uniform heat flux at the walls for the experimental study. An analytical model was developed. The temperature of the core fluid was assumed to vary in the vertical direction but not in horizontal direction. Recently Velusamy and Garg [9] given a numerical solution for the transient natural convection over heat generating vertical cylinders of various thermal capacities and radii. A fully implicit finite difference technique is used to solve nonlinear set of equations. The rate of propagation of the leading edge effect is given special consideration. They found that this rate, predicted by the one-dimensional conduction solution is slower than that resulting from the boundary layer solution. The transient boundary layer thickness is found to exceed its steady state values.

The unsteady natural convection flow over a vertical cylinder with MHD has given very scant attention in literature. Hence in the present study, the problem of unsteady free convection MHD flow of an incompressible viscous fluid, past a vertical cylinder, under the influence of a magnetic field is considered. The governing boundary layer equations along with the initial and boundary conditions are first cast into a dimensionless form and the resulting system of equations are then solved by an implicit finite difference scheme.

2. MATHEMATICAL ANALYSIS

The hydromagnetic flow of a viscous incompressible fluid past a vertical cylinder of radius r_0 with transversely applied magnetic filed is considered. Axial coordinate x is measured along the axis of the cylinder. The radial coordinate r is measured normal to the axis of the cylinder. The governing equations are expressed in terms of conservation of mass, momentum, energy, mass diffusion and the interaction of the flow with the magnetic field. All fluid properties are considered to be constant except for the density variation which induces the buoyancy force. The viscous dissipation is neglected in the energy equation. The concentration of the diffusing species in the binary mixture is very less in comparison to the other chem-

ical species, which are present. Hence, the interfacial velocity at the surface of the cylinder as the result of mass diffusion process is neglected. Also we assume that there is no chemical reaction between the diffusing species and the fluid. Initially the fluid and the cylinder are of same temperature T'_∞ and concentration C'_∞. At later time, the surface of the cylinder is raised to a uniform temperature T'_w and concentration C'_w. It is further assumed that the interaction of the induced axial magnetic field with the flow is considered to be negligible compared to the interaction of the applied magnetic field B_0, with the flow. Under these assumptions and Boussinesq's approximation, the flow is governed by the following system of equations:

$$\frac{\partial(ru)}{\partial x}+\frac{\partial(rv)}{\partial r}=0 \tag{1}$$

(continuity equation)

$$\frac{\partial u}{\partial t'}+u\frac{\partial u}{\partial x}+v\frac{\partial u}{\partial r}=g\beta\left(T'-T'_\infty\right)+g\beta^*\left(C'-C'_\infty\right)+\frac{\nu}{r}\frac{\partial}{\partial r}\left(r\frac{\partial u}{\partial r}\right)-\frac{\sigma B_0^2}{\rho}u \tag{2}$$

(momentum equation)

$$\frac{\partial T'}{\partial t'}+u\frac{\partial T'}{\partial x}+v\frac{\partial T'}{\partial r}=\frac{\alpha}{r}\frac{\partial}{\partial r}\left(r\frac{\partial T'}{\partial r}\right) \tag{3}$$

(energy equation)

$$\frac{\partial C'}{\partial t'}+u\frac{\partial C'}{\partial x}+v\frac{\partial C'}{\partial r}=\frac{D}{r}\frac{\partial}{\partial r}\left(r\frac{\partial C'}{\partial r}\right) \tag{4}$$

(mass diffusion equation)

with initial and boundary conditions

$$\begin{aligned}
t'\le 0:\quad & u=0, && v=0 && \\
& T'=T'_\infty, && C'=C'_\infty && \text{for all } x \text{ and } r\\
t'>0:\quad & u=0, && v=0 && \\
& T'=T'_w, && C'=C'_w && \text{at } r=r_0\\
& u=0, && T'=T'_\infty, && C'=C'_\infty \quad \text{at } x=0\\
& u\to 0, && T'\to T'_\infty, && C'\to C'_\infty \quad \text{as } r\to\infty
\end{aligned} \tag{5}$$

Introducing the following nondimensional quantities

$$X=Gr^{-1}\frac{x}{r_0},\qquad R=\frac{r}{r_0},\qquad U=\frac{ur_0Gr^{-1}}{\nu}$$

$$V=\frac{vr_0}{\nu},\qquad t=\frac{\nu t'}{r_0^2},\qquad T=\frac{T'-T'_\infty}{T'_w-T'_\infty}$$

$$C=\frac{C'-C'_\infty}{C'_w-C'_\infty},\qquad Gr=\frac{g\beta r_0^3(T'_w-T'_\infty)}{\nu^2} \tag{6}$$

$$Gr^*=\frac{g\beta^* r_0^3(C'_w-C'_\infty)}{\nu^2},\qquad Sc=\frac{\nu}{D}$$

$$N=\frac{Gr^*}{Gr},\qquad M=\frac{\sigma B_0^2 r_0^2}{\rho\nu},\qquad Pr=\frac{\nu}{\alpha}$$

equations (1)–(4) are reduced to the following form:

$$\frac{\partial(RU)}{\partial X}+\frac{\partial(RV)}{\partial R}=0 \tag{7}$$

$$\frac{\partial U}{\partial t}+U\frac{\partial U}{\partial X}+V\frac{\partial U}{\partial R}=T+NC+\frac{1}{R}\frac{\partial}{\partial R}\left(R\frac{\partial U}{\partial R}\right)-MU \tag{8}$$

$$\frac{\partial T}{\partial t}+U\frac{\partial T}{\partial X}+V\frac{\partial T}{\partial R}=\frac{1}{PrR}\frac{\partial}{\partial R}\left(R\frac{\partial T}{\partial R}\right) \tag{9}$$

$$\frac{\partial C}{\partial t}+U\frac{\partial C}{\partial X}+V\frac{\partial C}{\partial R}=\frac{1}{ScR}\frac{\partial}{\partial R}\left(R\frac{\partial C}{\partial R}\right) \tag{10}$$

The corresponding initial and boundary conditions in nondimensional quantities are given by

$$\begin{aligned}
t\le 0:\quad & U=0, && V=0 && \\
& T=0, && C=0 && \text{for all } X \text{ and } R\\
t>0:\quad & U=0, && V=0 && \\
& T=1, && C=1 && \text{at } R=1\\
& U=0, && T=0, && C=0 \quad \text{at } X=0\\
& U\to 0, && T\to 0, && C\to 0 \quad \text{as } R\to\infty
\end{aligned} \tag{11}$$

3. NUMERICAL TECHNIQUE

The governing equations are unsteady, coupled and nonlinear. Hence a numerical method must be employed to solve these equations. Here, an implicit finite difference method of Crank–Nicolson type is used to solve the governing equations. In the initial step, the partial differential equations (7)–(10) are converted into finite difference equations. They are as follows:

$$\begin{aligned}
&\frac{U^{k+1}_{i,j-1}-U^{k+1}_{i-1,j-1}+U^{k+1}_{i,j}-U^{k+1}_{i-1,j}}{4\Delta X}\\
&+\frac{U^{k}_{i,j-1}-U^{k}_{i-1,j-1}+U^{k}_{i,j}-U^{k}_{i-1,j}}{4\Delta X}\\
&+\frac{V^{k+1}_{i,j}-V^{k+1}_{i,j-1}+V^{k}_{i,j}-V^{k}_{i,j-1}}{2\Delta R}\\
&+\frac{V^{k+1}_{i,j}}{1+(j-1)\Delta R}=0
\end{aligned} \tag{12}$$

$$\frac{U_{i,j}^{k+1}-U_{i,j}^{k}}{\Delta t}+\frac{U_{i,j}^{k}}{2\Delta X}\left(U_{i,j}^{k+1}-U_{i-1,j}^{k+1}+U_{i,j}^{k}-U_{i-1,j}^{k}\right)$$
$$+\frac{V_{i,j}^{k}}{4\Delta R}\left(U_{i,j+1}^{k+1}-U_{i,j-1}^{k+1}+U_{i,j+1}^{k}-U_{i,j-1}^{k}\right)$$
$$=\frac{T_{i,j}^{k+1}+T_{i,j}^{k}}{2}+\frac{N(C_{i,j}^{k+1}+C_{i,j}^{k})}{2}$$
$$+\frac{U_{i,j-1}^{k+1}-2U_{i,j}^{k+1}+U_{i,j+1}^{k+1}+U_{i,j-1}^{k}-2U_{i,j}^{k}+U_{i,j+1}^{k}}{2(\Delta R)^{2}}$$
$$+\frac{U_{i,j+1}^{k+1}-U_{i,j-1}^{k+1}+U_{i,j+1}^{k}-U_{i,j-1}^{k}}{4[1+(j-1)\Delta R]\Delta R}$$
$$-\frac{M}{2}\left(U_{i,j}^{k+1}+U_{i,j}^{K}\right) \tag{13}$$

$$\frac{T_{i,j}^{k+1}-T_{i,j}^{k}}{\Delta t}+\frac{U_{i,j}^{k}}{2\Delta X}\left(T_{i,j}^{k+1}-T_{i-1,j}^{k+1}+T_{i,j}^{k}-T_{i-1,j}^{k}\right)$$
$$+\frac{V_{i,j}^{k}}{4\Delta R}\left(T_{i,j+1}^{k+1}-T_{i,j-1}^{k+1}+T_{i,j+1}^{k}-T_{i,j-1}^{k}\right)$$
$$=\frac{T_{i,j-1}^{k+1}-2T_{i,j}^{k+1}+T_{i,j+1}^{k+1}+T_{i,j-1}^{k}-2T_{i,j}^{k}+T_{i,j+1}^{k}}{2Pr(\Delta R)^{2}}$$
$$+\frac{T_{i,j+1}^{k+1}-T_{i,j-1}^{k+1}+T_{i,j+1}^{k}-T_{i,j-1}^{k}}{4Pr[1+(j-1)\Delta R]\Delta R} \tag{14}$$

$$\frac{C_{i,j}^{k+1}-C_{i,j}^{k}}{\Delta t}+\frac{U_{i,j}^{k}}{2\Delta X}\left(C_{i,j}^{k+1}-C_{i-1,j}^{k+1}+C_{i,j}^{k}-C_{i-1,j}^{k}\right)$$
$$+\frac{V_{i,j}^{k}}{4\Delta R}\left(C_{i,j+1}^{k+1}-C_{i,j-1}^{k+1}+C_{i,j+1}^{k}-C_{i,j-1}^{k}\right)$$
$$=\frac{C_{i,j-1}^{k+1}-2C_{i,j}^{k+1}+C_{i,j+1}^{k+1}+C_{i,j-1}^{k}-2C_{i,j}^{k}+C_{i,j+1}^{k}}{2Sc(\Delta R)^{2}}$$
$$+\frac{C_{i,j+1}^{k+1}-C_{i,j-1}^{k+1}+C_{i,j+1}^{k}-C_{i,j-1}^{k}}{4Sc[1+(j-1)\Delta R]\Delta R} \tag{15}$$

where the conventional notations are defined in the Nomenclature.

The region of integration is considered as a rectangle with sides $X_{\max}$ (= 1.0) and $R_{\max}$ (= 16) where $R_{\max}$ corresponds to $R = \infty$ which lies very well outside the momentum, thermal and concentration boundary layers.

The initial values of U, V, T and C are known from the initial boundary conditions. In the next time step, equations (12)–(15) constitute a tri-diagonal system of equations in the axial direction. While marching in axial direction, the interlinkage of momentum, energy and mass diffusion equations are retained. Such a system of equations are solved using Thomas algorithm as described by Carnahan et al. [10]. This iterative axial marching process is repeated for several time steps until steady state is reached. The steady state solution is assumed to be reached, when the absolute difference between the values of U, T and C at two consecutive time steps are less than 10^{-5} at each grid point.

After experimenting with a few set of mesh sizes, the mesh sizes are fixed at the level $\Delta X = 0.02$, $\Delta R = 0.20$ and $\Delta t = 0.01$. Spatial mesh sizes are reduced by 50 % in one direction and then in both directions and the results are compared. The results are found to be differing only in the fourth decimal place. Hence these mesh sizes are considered to be an appropriate for calculations.

The truncation error in the finite difference scheme is $O(\Delta t^2 + \Delta R^2 + \Delta X)$ and it tends to be zero as ΔX, ΔR, $\Delta t \to 0$. Hence the scheme is compatible. The finite difference scheme is unconditionally stable. Compatibility and stability ensures the convergence of the scheme.

4. RESULTS AND DISCUSSION

Computed temperature and concentration profiles are compared with the existing results of Chen and Yuh [5] for $Pr = 0.7$, $Sc = 0.2$, $N = 1.0$ and $M = 0.0$. It is observed that the present solution matches with the existing data closely as shown in the *figure 1*.

Figure 2 represents the velocity profiles at different time levels near the cylinder at $X = 1.0$. Velocity increases with time and reaches the steady state after certain lapse of time as shown in the *figure 2*. Temporal maximum is not observed. As Pr increases, the heat transfer rate increases. Hence the velocity decreases with increasing Pr. Time taken to reach steady state increases as Pr increases. When N, the combined ratio parameter, increases, velocity increases. The velocity profile decreases with increase in magnetic field parameter M. Time taken to reach the steady state increases as M increases.

In *figure 3* transient temperature profiles are shown for different parameters at $X = 1.0$. With increasing Pr, lower temperature profiles are observed, since the increasing Pr value gives higher heat transfer rates. This is due to the fact that higher the Pr, higher the heat transfer rates. With decreasing M, the magnetic field parameter, the temperature profiles are decreasing. Increasing temperature profiles are observed for decreasing N.

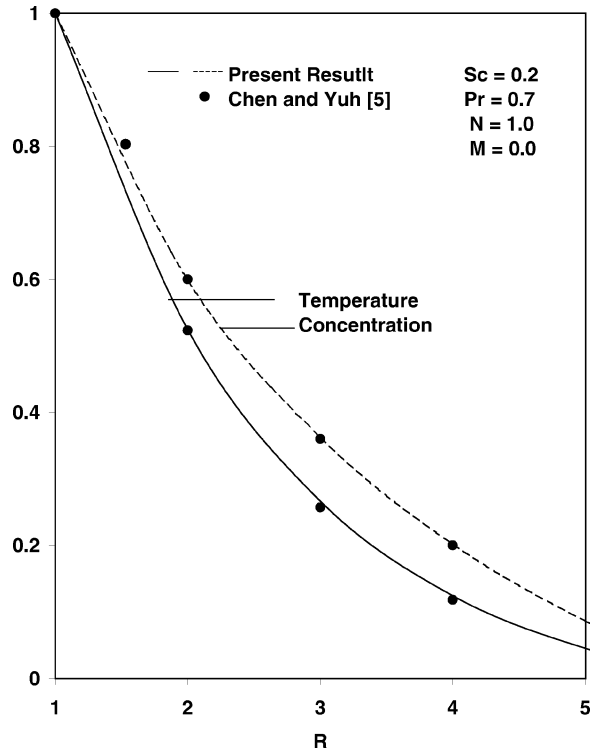

Figure 1. Comparison of temperature and concentration profile.

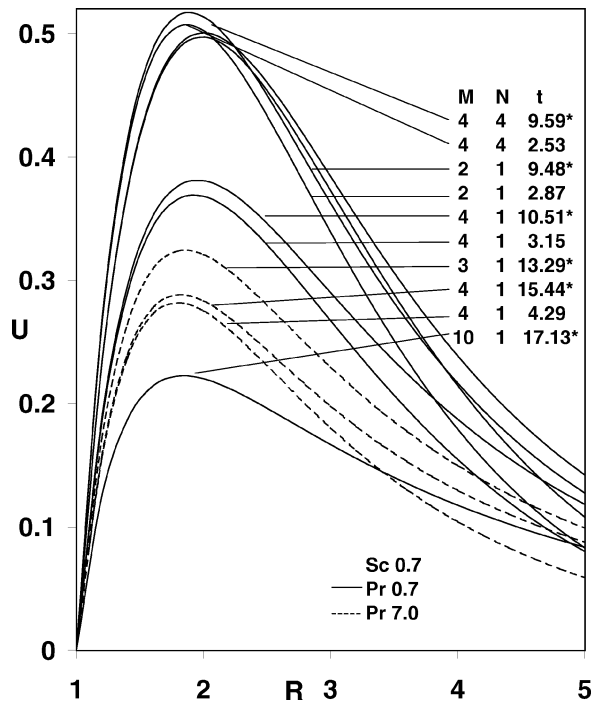

Figure 2. Transient velocity profiles at $X = 1.0$ (*—steady state).

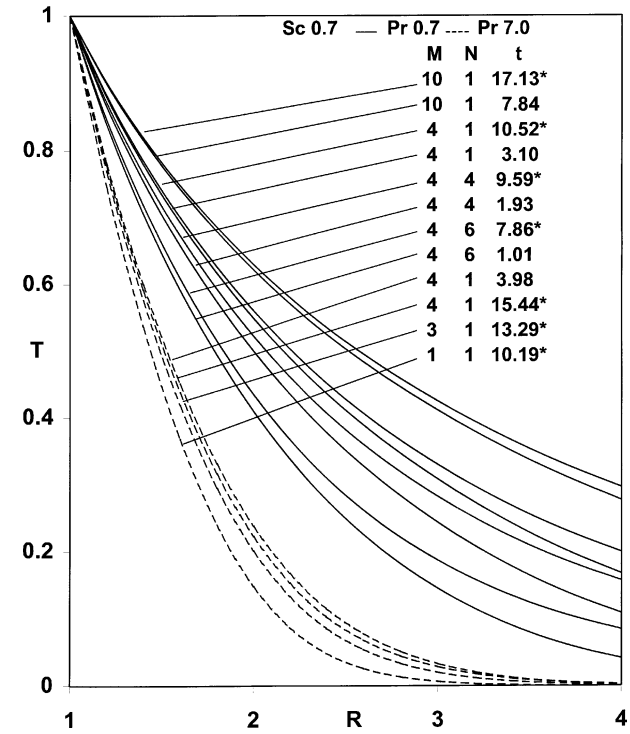

Figure 3. Transient temperature profiles at $X = 1.0$ (*—steady state).

Figure 4 represents unsteady concentration profiles. As *Sc* increases, the mass transfer rate increases. Hence, the concentration decreases with increasing *Sc*. The temporal maximum is observed for increasing values of *Sc*. In the case of increasing N, the combined buoyancy ratio parameter, the concentration profiles are observed to be decreasing. The same effect is observed for temperature profiles. As the magnetic field parameter increases the concentration profiles are increasing.

Knowing velocity, temperature and concentration profiles, it is interesting to study about the local and average values of skin-friction, Nusselt number and Sherwood number. In nondimensional quantities, they are given by

$$\tau_X = Gr\left(\frac{\partial U}{\partial R}\right)_{R=1} \tag{16}$$

$$\bar{\tau} = Gr\int_0^1 \left(\frac{\partial U}{\partial R}\right)_{R=1} \tag{17}$$

$$Nu_X = -Gr\left(\frac{\partial T}{\partial R}\right)_{R=1} \tag{18}$$

$$\overline{Nu} = -Gr\int_0^1 \left(\frac{\partial T}{\partial R}\right)_{R=1} \mathrm{d}X \tag{19}$$

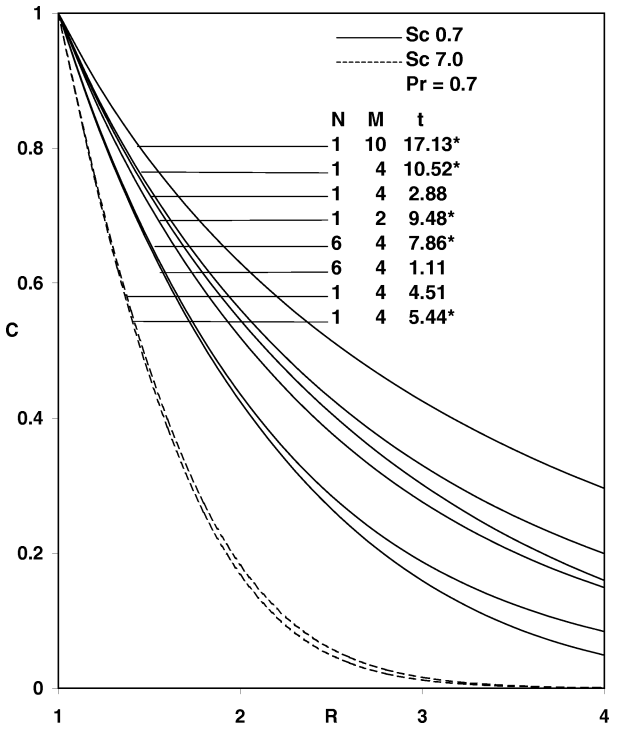

Figure 4. Transient concentration profiles at $X = 1.0$ (* – steady state).

$$Sh_X = -XGr\left(\frac{\partial C}{\partial R}\right)_{R=1} \tag{20}$$

$$\overline{Sh} = -Gr\int_0^1 \left(\frac{\partial C}{\partial R}\right)_{R=1} \mathrm{d}X \tag{21}$$

The derivatives involved in equations (16)–(21) are evaluated by using a five-point approximation formula and then the integrals are evaluated by using Newton–Cotes closed integration formula.

In *figure 5* local skin friction at steady state are plotted for different values of parameters against the axial co-ordinate X. It increases as X increases. As N increases, local skin-friction increases. Local skin-friction decreases with increasing *Pr* or *Sc*. This is due to the fact that increasing *Pr* and *Sc* gives rise to higher heat and mass transfer rate, respectively. Lower values of magnetic field parameter lead to higher values of local skin friction.

Steady state local Nusselt number results are plotted in *figure 6*. It increases as X increases. The effect of *Pr* is more on local Nusselt number than any other parameter. It decreases when M increases or N decreases.

Steady state local Sherwood number are plotted in *figure 7*. The mass transfer rate increases as *Sc* increases.

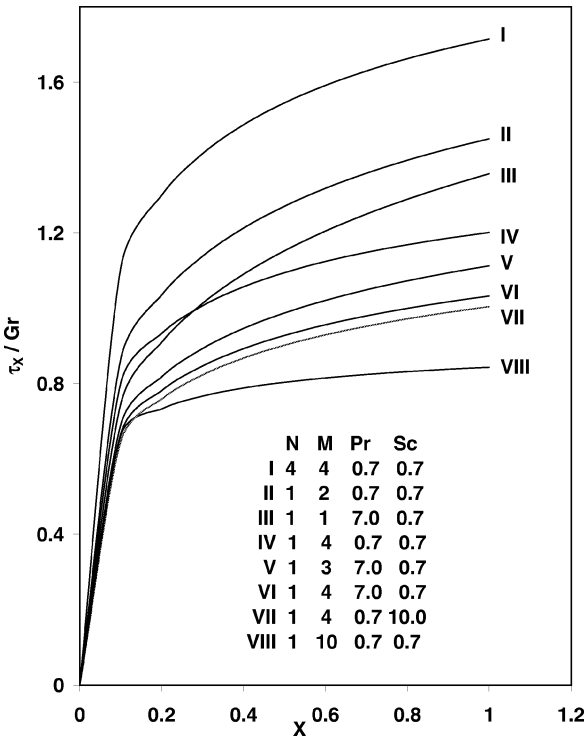

Figure 5. Local skin-friction.

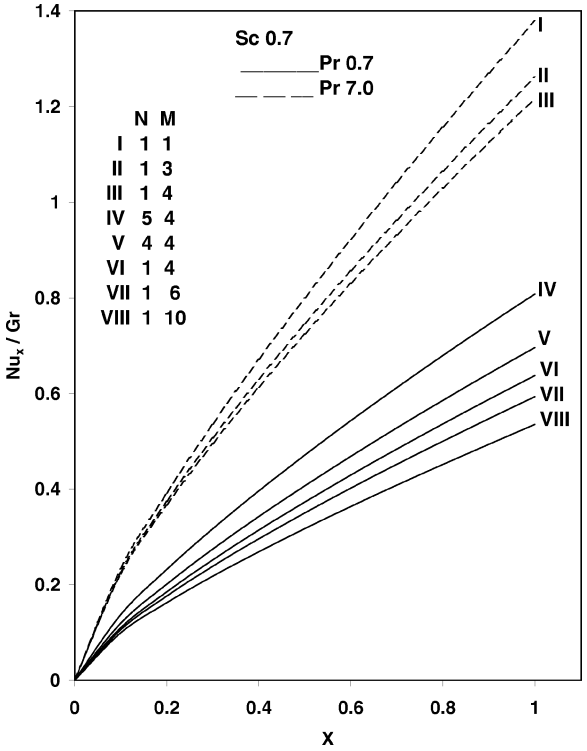

Figure 6. Local Nusselt number.

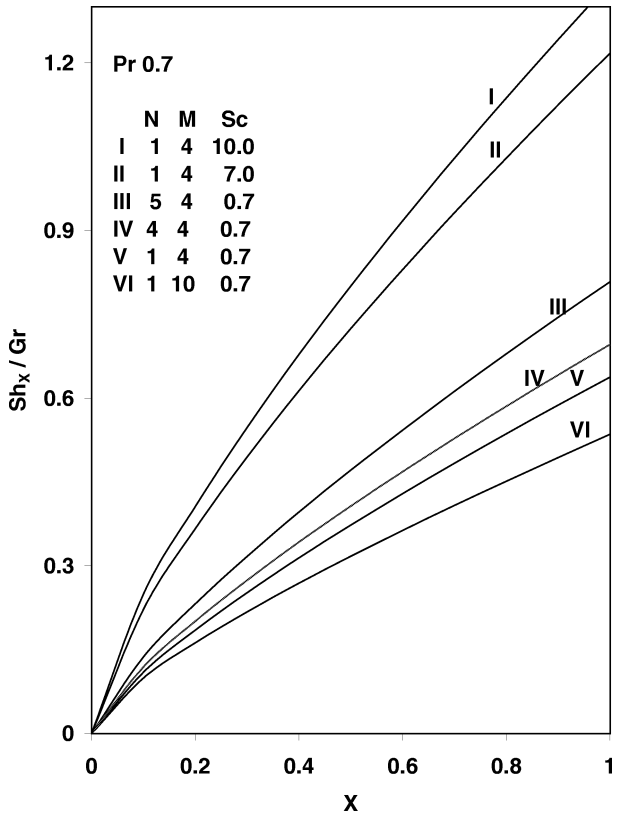

Figure 7. Local Sherwood number.

Hence, larger values of local Sherwood number are observed for increasing *Sc*. As *M* increases it decreases. For increasing values of *N* larger local Sherwood number is observed.

Average values of skin friction, Nusselt number and Sherwood number are plotted for various parameters in *figures 8*, *9* and *10*, respectively. Average values of skin friction get reduced with increasing values of *Sc* or *M* throughout the transient period and steady state level. *Figure 9* shows that there is no change in *Nu*, in the initial period with respect to *Pr*. This reveals that heat transfer is due to conduction. For increasing values of *N*, the average Nusselt number increases. It decreases as the magnetic parameter increases. *Figure 10* shows that, at small times, for fixed *Sc*, the average Sherwood number is constant for various parameters. This is due to the fact that only pure mass diffusion takes place during this time. It is also observed that an increase in *M* reduces the average Sherwood number values.

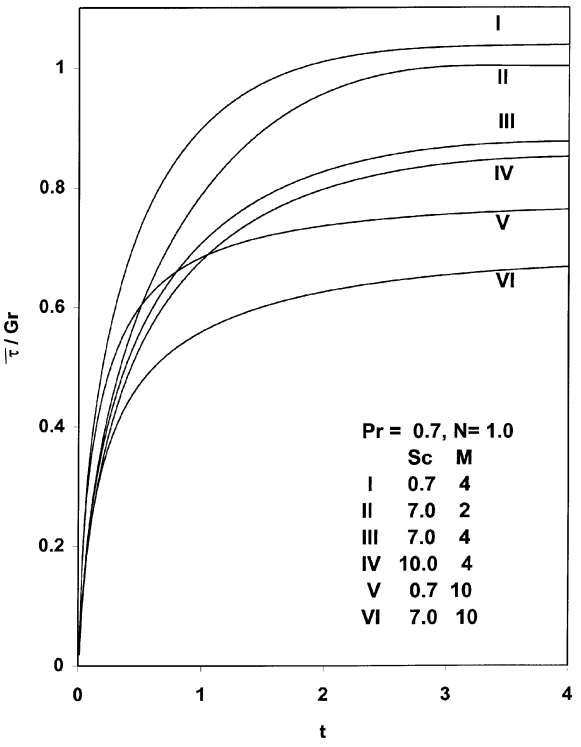

Figure 8. Average skin-friction.

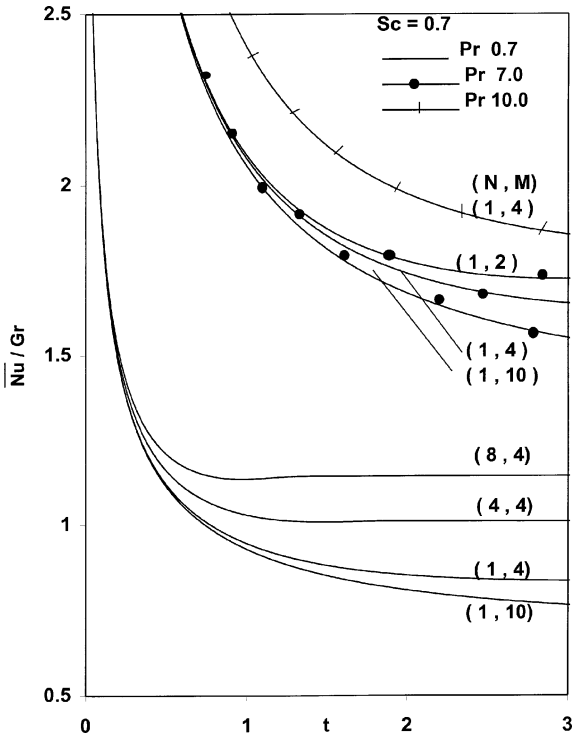

Figure 9. Average Nusselt number.

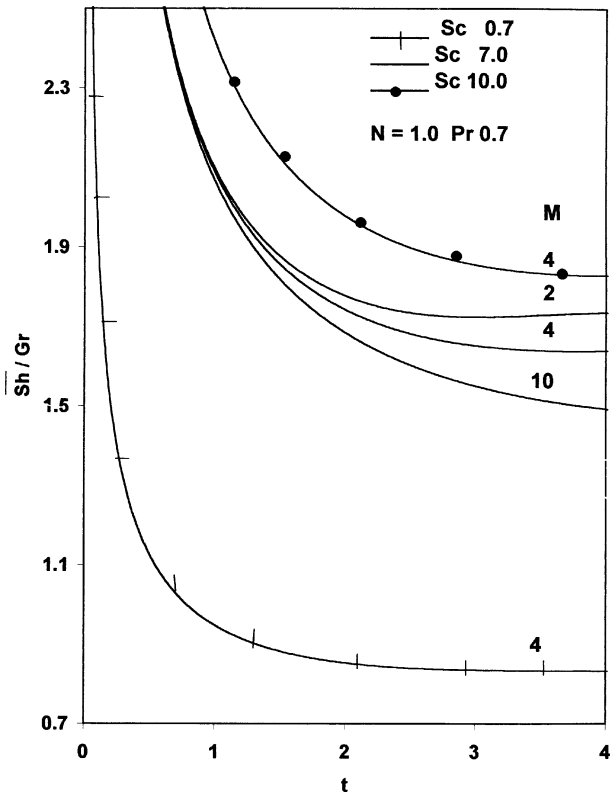

Figure 10. Average Sherwood number.

Acknowledgement

The authors wished to acknowledge support for this research work from CSIR (Council of Scientific and Industrial Research) through the sanction of Research Grant.

REFERENCES

[1] Agrawal A.K., Samria N.K., Gupta S.N., Combined buoyancy effects of thermal and mass diffusion on hydromagnetic visco-elastic natural convection flow past an accelerated infinite plate, J. En. Heat Mass Tran. 20 (1998) 35–42.

[2] Helmy K.A., MHD unsteady free convection flow past a vertical porous plate, ZAMM 78 (1998) 255–270.

[3] Jones O.S., Shumlak U., Eberhardt D.S., An implicit scheme for non-ideal magnetohydrodynamics, J. Comput. Phys. 130 (1997) 231–242.

[4] Shanker B., Kishan N., The effects of mass transfer on the MHD flow past an impulsively started infinite vertical plate with variable temperature or constant heat flux, J. En. Heat Mass Tran. 19 (1997) 273–278.

[5] Chen T.S., Yuh C.F., Combined heat and mass transfer in natural convection along a vertical cylinder, Int. J. Heat Mass Tran. 23 (1980) 451–461.

[6] Goldstein R.J., Briggs D.G., Transient free convection about vertical plates and circular cylinders, J. Heat Tran. 86 (1964) 490–500.

[7] Dring R.P., Gebhart B., Transient natural convection from thin vertical cylinders, Trans. ASME J. Heat Tran. 88 (1996) 246–247.

[8] Evan L.B., Reid R.C., Drake E.M., Transient natural convection in a vertical cylinder, A.I.Ch.E.J. 14 (1968) 251–261.

[9] Velusamy K., Garg V.K., Transient natural convection over a heat generating vertical cylinder, Int. J. Heat Mass Tran. 35 (1992) 1293–1306.

[10] Carnahan B., Luther H.A., Wilkes J.O., Applied Numerical Methods, Wiley, New York, 1969.